

# Breaking Rayleigh's curse for two unbalanced single-photon emitters: BLESS technique

Konstantin Katamadze\*

Valiev Institute of Physics and Technology, Russian Academy of Sciences, 117218, Moscow, Russia and  
Quantum Technology Centre, Faculty of Physics, M. V. Lomonosov Moscow State University, 119991, Moscow, Russia

Boris Bantysh, Andrey Chernyavskiy, and Yurii Bogdanov

Valiev Institute of Physics and Technology, Russian Academy of Sciences, 117218, Moscow, Russia

Sergei Kulik

Quantum Technology Centre, Faculty of Physics, M. V. Lomonosov Moscow State University, 119991, Moscow, Russia

(Dated: May 21, 2024)

Rayleigh's criterion posits that resolving point sources below point spread function width is impossible. Statistical estimation overcomes this but suffers from increasing error at shorter distances, known as Rayleigh's curse. Target mode shaping solves this for equal sources but not for multi-parameter objects like emitters with unknown brightness ratio. We propose BLESS technique, utilizing Beam modulation and Examination of Shot Statistics, breaking Rayleigh's curse for unbalanced sources. Demonstrated through classical and quantum Cramér–Rao bound calculations, BLESS shows significant potential for real imaging experiments.

**Introduction.**— Fluorescent microscopy is essential for many biological applications. It uses dye molecules or quantum dots that emit photons to create images. The Rayleigh limit dictates that two emitters cannot be resolved if the distance between them is smaller than the point spread function (PSF) width  $\sigma$ , which is proportional to the wavelength  $\lambda$  [1].

To overcome this limit, several techniques have been developed, such as STED [2], which utilizes donut-mode laser illumination to selectively deplete luminescence, effectively reducing the effective PSF width. Another approach employed in STORM [3] and PALM [4] relies on temporally switching off molecules, causing them to blink one by one for precise localization. However, when simultaneous photon emission occurs from two nearby sources, estimating the distance  $d$  between them becomes challenging, particularly when  $d < \sigma$ , the distance estimation error  $\Delta_d$  increases polynomially with distance decrease, known as Rayleigh's curse [5].

By evaluating quantum Fisher information (QFI), Tsang et al. demonstrated the possibility of overcoming Rayleigh's curse for two *equal* point sources [5–7]. They showed that QFI is independent of the distance  $d$ , enabling precise estimation beyond the Rayleigh limit. Practical measurement protocols like SPADE [5] and SLIVER [6] nearly achieve the QFI limit by shaping the target mode to transform the effective PSF. While demonstrated in proof-of-principle experiments [8–12], these methods have not been applied in real imaging applications where sources are *unequal* and have varying brightness. Subsequent studies showed that Rayleigh's curse persists for unbalanced sources with unknown brightness ratio [13, 14].

To achieve precise imaging of complex objects, additional information can be gleaned from the photon statistics examination. Photon correlation measurements have already been utilized for resolution enhancement [15–21]

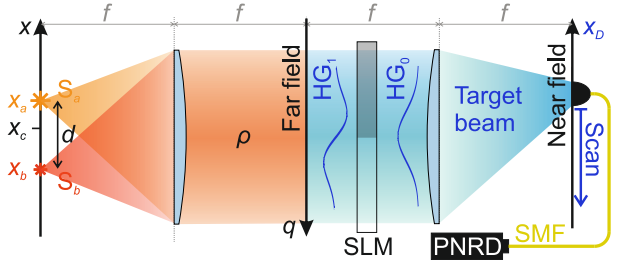


FIG. 1. The principal imaging scheme. SLM – spatial light modulator, SMF – single-mode fiber, PNRD – photon number resolving detector.

and for subdiffraction localization of single-photon emitters [22–25]. However, to our knowledge, this approach has not been combined with target mode shaping, and overcoming Rayleigh's curse has not been demonstrated yet.

In this work, we introduce a pioneering imaging method named BLESS (Beam modulation and Estimation of Shot Statistics). We show that in contrast to direct imaging and SLIVER/SPADE techniques, it represents the first instance of overcoming Rayleigh's curse for a general problem involving two unbalanced single-photon emitters with unknown brightness ratio. Additionally, we validate its effectiveness in practical imaging situations by considering experimentally feasible parameters and addressing major imperfections in imaging systems.

**Theoretical model.**— Consider a 1D imaging problem for two uncorrelated and non-interfering single-photon point sources  $S_a$  and  $S_b$  located at  $x_a$  and  $x_b$  respectively (Fig. 1). The sources have the following photon number  $n$  distributions:

$$P_s(n) = \delta_{0n}(1 - \mu_s) + \delta_{1n}\mu_s, \quad s = a, b \quad (1)$$

where  $\delta_{ij}$  is the Kronecker delta and  $\mu_s \in [0, 1]$  is a mean

photon number. One can describe this object using the following set of four parameters:

- distance  $d = x_a - x_b$ ,
- total mean photon number  $\mu = \mu_a + \mu_b$ ,
- centroid  $x_c = (\mu_a x_a + \mu_b x_b) / \mu$ ,
- relative brightness  $\gamma = (\mu_a - \mu_b) / \mu \in [-1, 1]$ .

The light from the source is passed through a  $4f$  imaging system with 1:1 magnification. Since any far-field imaging system has a limited numerical aperture (NA), it results in the loss of photons and information about the source position. Typically, NA can be approximated with a Gaussian function, so that the light from the source  $S_s$ , located at  $x_s$  ( $s = a, b$ ), exhibits a Gaussian far-field electric field distribution over the transverse wave vector component  $\Psi_s(q) = \text{HG}_0(q, \sigma) e^{-iqx_s}$ , where

$$\text{HG}_m(q, \sigma) \equiv \sqrt{\frac{\sigma}{\sqrt{\pi} 2^m m!}} e^{-\frac{im\pi}{2}} e^{-\frac{\sigma^2 q^2}{2}} H_m(\sigma q) \quad (2)$$

is a standard definition of the Hermite-Gaussian mode in a far-field. In the near-field  $\Psi_s(q)$  is related to the Gaussian PSF  $\tilde{\Psi}_s(x) = \frac{1}{\sqrt{\pi} \sigma} e^{-\frac{(x-x_s)^2}{2\sigma^2}}$  with  $\sigma \sim \lambda/\text{NA}$ .

In the image plane, light is coupled to the single-mode fiber (SMF) collimator which forms a Gaussian target (detection) mode centered at  $x_D$  with waist  $\sigma_D$ :  $\Phi_0(q) = \text{HG}_0(q, \sigma_D) e^{-iqx_D}$ . Here and below lower index  $D$  corresponds to the detection process. Scanning  $x_D$  one can measure the image profile. Additionally, one can place a spatial light modulator (SLM) between the lenses which transforms the Gaussian  $\text{HG}_0$  Target Mode into the first Hermite-Gaussian mode  $\text{HG}_1$  with the field distribution  $\Phi_1(q) = \text{HG}_1(q, \sigma_D) e^{-iqx_D}$ . Below we will show that this target beam modulation combined with a photon number distribution measurement plays a key role in precise emitter localization.

In order to measure the photon number distribution, the SMF output is connected to a photon number resolving detector (PNRD). For simplicity, we assume the detector quantum efficiency to be 100%. The probability of detecting a single photon emitted by the point source  $S_s$  in the  $\Phi_m$  target mode ( $m = 0, 1$ ) is then

$$T_s^{(m)} = \left| \int \Phi_m^*(q) \Psi_s(q) dq \right|^2 = \xi^m e^{-\xi}, \quad s = a, b, \quad (3)$$

where  $\xi \equiv \frac{(x_s - x_D)^2}{2\sigma^2}$ . Here and below we consider the case  $\sigma_D = \sigma$  to mode-match the target mode with the PSF.

Then the total probability  $P_{s,D}^{(m)}(k)$  of detecting  $k$  photons from the source  $S_s$  is just the convolution of the initial photon number distribution  $P_s(n)$  with the binomial distribution having a success probability  $T_s^{(m)}$ . Since the sources are uncorrelated and non-interfering, the convolution of  $P_{a,D}^{(m)}$  and  $P_{b,D}^{(m)}$  gives the detected photon number

distribution  $P_D^{(m)}(k|\theta, x_D)$ , which depends on the detector position  $x_D$  and object parameters  $\theta = \{d, \gamma, x_c, \mu\}$ :

$$P_D^{(m)}(0|\theta, x_D) = (1 - M_a^{(m)})(1 - M_b^{(m)}), \quad (4a)$$

$$P_D^{(m)}(1|\theta, x_D) = M_a^{(m)} + M_b^{(m)} - 2M_a^{(m)}M_b^{(m)}, \quad (4b)$$

$$P_D^{(m)}(2|\theta, x_D) = M_a^{(m)}M_b^{(m)}, \quad (4c)$$

where  $M_s^{(m)} \equiv \mu_s T_s^{(m)}$ . The probability to detect more than two photons from two emitters equals zero. The mean detected photon number  $\langle k \rangle$  for this distribution is

$$M_D^{(m)}(x_D) = M_a^{(m)} + M_b^{(m)}, \quad (5)$$

the variance  $\langle k^2 \rangle - \langle k \rangle^2$  is

$$V_D^{(m)}(x_D) = M_a^{(m)}(1 - M_a^{(m)}) + M_b^{(m)}(1 - M_b^{(m)}), \quad (6)$$

and the normalized second-order correlation function at the zero time-delay  $\langle k(k-1) \rangle / \langle k \rangle^2$  is

$$g_D^{(m)}(x_D) = \frac{2M_a^{(m)}M_b^{(m)}}{(M_a^{(m)} + M_b^{(m)})^2}. \quad (7)$$

*Main idea.*— Target mode shaping methods [5–7, 13, 14] efficiently estimate the distance  $d$  between two equal sources but stumble when dealing with sources of unknown relative brightness  $\gamma$ . This difficulty arises from their inability to measure these two parameters separately. However, by independently estimating  $\gamma$  from photon statistics measurements, we can overcome this limitation, thereby enabling the breaking of Rayleigh's curse even for unbalanced sources.

Indeed, for two close ( $d \ll \sigma$ ) emitters, the mean photon number profile (5) in the  $\text{HG}_1$  target mode centered near the centroid location  $x_c$  can be approximated as (see Fig.2):

$$M_D^{(1)}(x_D) \approx \frac{\mu}{2\sigma^2} \left[ (x_D - x_c)^2 + \frac{gd^2}{2} \right], \quad (8)$$

where  $g \equiv 1 - \gamma^2$  equals the total second-order correlation function of the sources (Eq.(7) with  $T_a = T_b = 1$ ).

Using (S10) the distance is estimated from the measured value  $M_{x_c} \equiv M_D^{(1)}(x_D = x_c)$  as  $d = 2\sigma \sqrt{M_{x_c}/(\mu g)}$ ,

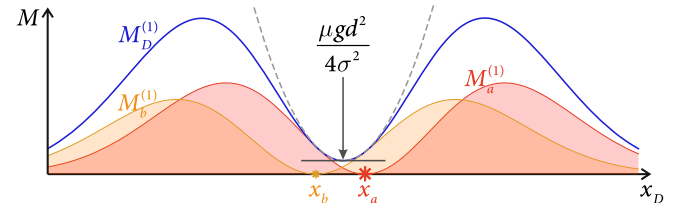


FIG. 2. The image with  $\text{HG}_1$  PSF. The filled orange and red curves correspond to mean photon numbers  $M_a^{(1)}$  and  $M_b^{(1)}$  in the target mode from the sources  $S_a$  and  $S_b$ . The blue curve – total detected mean photon number  $M_D^{(1)} = M_a^{(1)} + M_b^{(1)}$ . Dashed curve – its approximation (S10).

where  $x_c$  and  $\mu$  are preliminarily estimated by direct imaging, and  $g$  is independently estimated from photon statistics measurements. In this scenario, one can show (see Supplementary [26]) that the distance estimation error (standard deviation of the estimated value) is given by:

$$\Delta_d \approx \frac{d}{2\sqrt{M_{x_c}K}} = \frac{\sigma}{\sqrt{\mu g K}}, \quad (9)$$

where  $K$  denotes the number of measurements.

Moreover, photon statistics measured in the  $\text{HG}_0$  mode also provide the means to estimate both  $d$  and  $\gamma$ . By defining  $P_{2\pm}$  as the probability of detecting two photons at  $x_D = \pm\sigma$ , one estimates  $g \approx 2e^{\frac{P_{2+}+P_{2-}}{\mu^2}}$ , while  $\gamma$  is obtained as  $\gamma = \pm\sqrt{1-g}$ . The distance is then estimated as  $d = 2\frac{x_c}{\gamma} - \frac{2e\sigma}{\mu^2 g \gamma}(P_{2+} - P_{2-})$ . Giving known values of  $x_c$ ,  $\gamma$ , and  $\mu$ , the distance estimation error is (see Supplementary [26]):

$$\Delta_d \sim \frac{\sigma}{\mu \gamma \sqrt{g K}}. \quad (10)$$

Since both  $\Delta_d$  estimation errors (9) and (10) do not depend on  $d$ , estimation of shot statistics allows one to break Rayleigh's curse for both  $\text{HG}_0$  and  $\text{HG}_1$  target modes. However, employing  $\text{HG}_1$  mode reduces  $\Delta_d$  by a factor of  $\gamma\sqrt{\mu}$ , enhancing accuracy.

**Errors bounds.**— For more accurate calculation of parameters' estimation errors for different measurement protocols we use the Cramér–Rao bound (CRB) theory [27, 28]. Consider an unbiased estimate  $\tilde{\theta}$  of four image parameters  $d$ ,  $\gamma$ ,  $x_c$ , and  $\mu$ . For each imaging experiment,  $\tilde{\theta}$  is a random vector centered at point  $\theta^*$  of the true parameters values [27, 28]. According to CRB, the covariance matrix  $\Sigma$  of  $\tilde{\theta}$  is bounded by the inverse of the positive semidefinite Fisher information matrix (FIM)  $F$ .

In the photon statistics measurement regime,  $F_m^{\text{stat}}(x_D) = \sum_k [\nabla_{\theta} P_D(k)] [\nabla_{\theta} P_D(k)]^T / P_D(k)$ , where  $P_D(k)$  is the photon-counts distribution (4), depended on  $\theta$  and known target mode parameters: position  $x_D$  and  $\text{HG}_m$  mode index  $m$ . In the mean photon number measurement regime, one extracts the information from the mean photon number  $M_D^{(m)}$  (5) having variance  $V_D^{(m)}$  (6). For normal statistical errors,  $F_m^{\text{mean}}(x_D) = [\nabla_{\theta} M_D^{(m)}] [\nabla_{\theta} M_D^{(m)}]^T / V_D^{(m)}$ .

Depending on measurement protocol the values  $\Delta_{\theta_\alpha} = \sqrt{[F^{-1}]_{\alpha\alpha}}$  describe the statistical limits of the parameters  $\theta_\alpha$  estimation errors. We evaluate these limits for four measurement protocols:

- **Direct Imaging (DI):** Sequentially measures the mean photon number in the  $\text{HG}_0$  mode at mesh points  $x_D = \{-1, -0.8, -0.6, \dots, 0.8, 1\}\sigma$ . It efficiently estimates mean photon number  $\mu$  and centroid  $x_c$  but fails to precisely estimate  $\gamma$  and  $d$ .

- **SPADE:** Consists of two stages; the first is equivalent to DI, while the second measures the mean photon number in the  $\text{HG}_1$  mode at point near  $x_c$ . Both stages take the same amount of time and allow for estimation of the product  $gd^2$  but not separately estimating  $g$  (or  $\gamma$ ) and  $d$ .

- **Examination of Shot Statistics (ESS):** Similar to DI but measures full photon statistics at each point. In addition to  $\mu$  and  $x_c$ , it enables estimation of  $g$  (or  $\gamma$ ) and  $d$  separately.

- **BLESS:** Consists of two stages; the first is similar to ESS, the second (as SPADE) measures mean photon number in the  $\text{HG}_1$  mode near  $x_c$  to enhance  $d$  estimation precision. Measuring photon statistics in the second stage doesn't offer any benefits.

**Quantum limit.**— The Fisher information matrix (FIM) depends on the particular measurement setting. However, one might be interested in the ultimate limit over all possible measurements. This could be achieved by computing the quantum Fisher information matrix (qFIM) [5, 29, 30]:

$$Q_{\alpha\beta} = 2 \sum_{kl, \lambda_k + \lambda_l \neq 0} \frac{\langle \psi_k | \partial_\alpha \hat{\rho} | \psi_l \rangle \langle \psi_l | \partial_\beta \hat{\rho} | \psi_k \rangle}{\lambda_k + \lambda_l} \Big|_{\theta=\theta^*}. \quad (11)$$

Here,  $\hat{\rho}$  is the image density operator, and  $\hat{\rho} = \sum_j \lambda_j |\psi_j\rangle\langle\psi_j|$  – its spectral decomposition. For any measurement setting,  $F \leq Q$ . In the general case of multi-parameter estimation, one can hardly find a particular measurement that satisfies  $F = Q$  [30]. However, below we will show that the proposed BLESS protocol is close to this limit.

The density operator of the field after the lens (in the far-field) produced by the single-photon source  $S_s$  with a mean photon number  $\mu_s$  is

$$\hat{\rho}_s = (1 - \mu_s) |vac\rangle\langle vac| + \mu_s |\Psi_s\rangle\langle\Psi_s|, \quad s = a, b. \quad (12)$$

Here  $|\Psi_s\rangle = \int dq \Psi_s(q) \hat{a}^\dagger(q) |vac\rangle$ , and  $\hat{a}^\dagger(q)$  creates one photon in a plane wave with the transverse wave vector  $q$ .

In the previous works, studying quantum Fisher Information for unbalanced emitters [13, 14, 31], authors used a weak source approximation  $\mu_s \ll 1$  and considered the density operator of the field produced by the two sources as

$$\hat{\rho}_1 = (1 - \mu_a - \mu_b) |vac\rangle\langle vac| + \mu_a |\Psi_a\rangle\langle\Psi_a| + \mu_b |\Psi_b\rangle\langle\Psi_b|. \quad (13)$$

This state carries at most one photon, so the quantum CRB, calculated from this quantum state will be referred to as qCRB-1. The state  $\hat{\rho}_1$  cannot provide any information about photon statistics. One may argue that for weak sources, the probability of detecting two photons vanishes, and thus measuring photon distribution does not provide any additional information. However, rare events may carry much information (e.g. consider measurements in

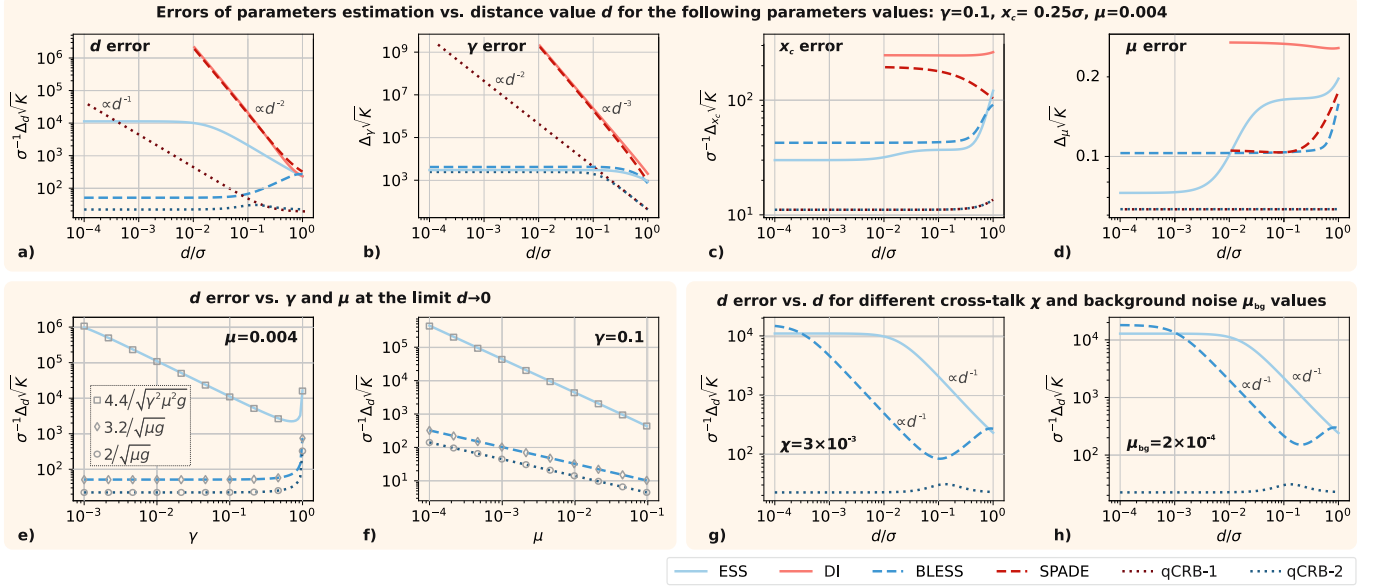


FIG. 3. Normalized estimation errors  $\Delta d$ ,  $\Delta \gamma$ ,  $\Delta x_c$ ,  $\Delta \mu$ , calculated using Cramér–Rao bound (CRB) for all the measurement protocols (BLESS, ESS, SPADE, DI), and quantum limits for the single-photon quantum state  $\hat{\rho}_1$  (qCRB-1) and two-photon state  $\hat{\rho}_2$  (qCRB-2). For all the plots  $\mu = 0.004$ ,  $x_c = 0.25\sigma$ ,  $\gamma = 0.1$ . (a–d) Errors for all four parameters vs.  $d$ . The lines for DI and SPADE start at  $d/\sigma = 10^{-2}$  since for smaller values corresponding FIMs become close to singular and cannot be numerically inverted. (e–f) Dependencies of  $\Delta d$  at the limit ( $d \rightarrow 0$ ) on  $\gamma$  and  $\mu$  for the bounds, which don’t diverge. Numerical values calculated for  $d = 10^{-4}\sigma$  are presented by curves. Squares, diamonds and circles correspond to analytical approximations, presented in the inset. (g, h) Impact of target mode shaping cross-talk ( $\chi = 3 \times 10^{-3}$ ) and background noise ( $\mu_{bg} = 2 \times 10^{-4}$ ).

PSF zeros [32], large amplification of weak values [33], or orthogonal measurements in quantum tomography [34]), so accounting for two-photon component might be crucial.

Thus, we define the full state as follows. For sources  $S_a$  and  $S_b$ , one can introduce two orthogonal subspaces and write down the density operator as the following mixture of the single-photon sources states (12):

$$\hat{\rho}_2 = \frac{1}{2}(\hat{\rho}_a \otimes \hat{\rho}_b + \hat{\rho}_b \otimes \hat{\rho}_a). \quad (14)$$

This form guarantees that the sources are incoherent and that one cannot filter out a single source and estimate its parameters separately. The quantum CRB, calculated from this state, will be referred to as qCRB-2. Below, we will demonstrate that the state  $\hat{\rho}_2$  indeed breaks Rayleigh’s curse even for small  $\mu$ , while  $\hat{\rho}_1$  doesn’t. Details of the state (14) derivation and the computation of the corresponding qFIM are described in Supplementary [26].

*Experimental imperfections.*— We address two main experimental imperfections. Firstly, non-ideal spatial modulation arises from imperfections in SLM and optical aberrations, leading to cross-talk  $\chi$  between  $HG_0$  and  $HG_1$  modes. Secondly, we consider background radiation with a Poissonian photon number distribution, characterized by mean photon number  $\mu_{bg}$ . Both imperfections lead to changes in the registered photon number distribution  $P_D^{(m)}(k)$  (4) (see details in Supplementary [26]).

Other imperfections like optical losses and non-unit PNRD efficiency are captured in parameter  $\mu$ , representing mean *registered* photon number. While assuming identical spectral and polarization properties, our technique doesn’t rely on photon interference between sources. Therefore, if sources can be distinguished by other means, it simplifies localization. Additionally, we limit consideration to one dimension, as the problem is well dimension-factorisable for two sources.

*Results and discussion.*— Since many fluorescent microscopy techniques were first tested on stable samples e.g. color centers in diamond, to evaluate our approach, we simulated conditions resembling real imaging scenario, where the objective is to resolve two nearby NV-centers. Previous studies [18, 35] demonstrate that a single NV-center can yield a detected count rate of up to 200 kcps, corresponding to the mean photon number value  $\mu_s \approx 2 \times 10^{-3}$  given its lifetime of approximately  $\tau = 10$  ns. Hence, for two close NV-centers, we chose a total mean photon number  $\mu = 4 \times 10^{-3}$ . Other model parameters were set as  $\gamma = 0.1$  and  $x_c = 0.25\sigma$  (to significantly shift  $x_c$  from the mesh points). Considering background radiation, we referred to the work [35], where it amounted to approximately 20 kcps ( $\mu_{bg} \approx 2 \times 10^{-4}$ ). The cross-talk between spatial modes was set at  $\chi = 3 \times 10^{-3}$  [36]. We present the Cramér–Rao bounds (CRBs) for all measurement pro-

protocols (BLESS, ESS, SPADE, DI) and the quantum CRBs (qCRB-1 and qCRB-2) for the single-photon state  $\hat{\rho}_1$  (13) and two-photon state  $\hat{\rho}_2$  (14) in Fig 3.

As depicted in Fig 3 (c,d), the centroid and total mean photon number estimation errors  $\Delta_{x_c}$  and  $\Delta_\mu$  are quite small and do not increase with decreasing  $d$ . Some step-like features in the ESS plots are observed, but they are not significant.

Estimating  $d$  and  $\gamma$  is more challenging. As shown in Fig 3 (a,b), for a single-photon qCRB-1  $\Delta_d \propto d^{-1}$  and  $\Delta_\gamma \propto d^{-2}$ , and for direct imaging (DI)  $\Delta_d \propto d^{-2}$  and  $\Delta_\gamma \propto d^{-3}$ , consistent with [14]. In contrast to the equal sources scenario, the SPADE protocol doesn't saturate qCRB-1 and works similarly to DI.

However, accounting for two-photon events qualitatively enhances the reachable resolution. Quantum CRB, based on the state  $\hat{\rho}_2$  (qCRB-2), as well as CRBs for protocols ESS and BLESS, based on photon statistics measurements, are independent of  $d$  for both  $\Delta_d$  and  $\Delta_\gamma$  estimation errors. This clearly demonstrates that this approach allows breaking Rayleigh's curse. Moreover, target mode modulation decreases the distance estimation error  $\Delta_d$  by a factor of  $\sim \gamma\sqrt{\mu}$ . Consequently, the BLESS protocol almost saturates the ultimate bound qCRB-2 (which remains independent of  $d$  except for a small peak at  $d \approx 0.1$ ; we cannot fully explain this peak, but it appears insignificant).

To demonstrate the protocols efficiency for various model parameters, we present dependencies of  $\Delta_d$  on  $\gamma$  and  $\mu$  in the limit  $d \rightarrow 0$ , as well as their analytical approximations under assumptions  $x_c \ll \sigma$ ,  $\mu \ll 1$  (similar to (9, 10), but with the fitted factor) in Fig 3 (e,f). Analytical approximations for error bounds of the other parameters can be found in Supplementary [26]. An interesting and counterintuitive feature of the ESS protocol is noted: for  $\gamma < 1/\sqrt{2}$ , more unbalanced sources can be resolved better, consistent with Eq. (10), derived from statistical error propagation theory.

The impact of cross-talk  $\chi$  and background noise  $\mu_{bg}$  is shown in Fig 3 (g,h). We found that they may significantly decrease the efficiency of the BLESS protocol. For  $d \gg 2\sigma\sqrt{\frac{\mu_{bg} + \mu\chi}{\mu g}}$ , the experimental imperfections are negligible. However, with continuous decrease in  $d$ , its estimation error grows inversely proportional to  $d$  until it reaches the bound for the ESS protocol, which is robust to both imperfection types (see details in Supplementary [26]).

While our primary focus has been on the fundamental problem of breaking Rayleigh's curse, it is practically reasonable to estimate the exposure time required to resolve two separated sources (achieving  $\Delta_d \leq d$ ). We define  $\alpha = \sigma/d$  as a resolution enhancement w. r. t. the Rayleigh limit. Figures 3 (a,g,h) show the normalized distance estimation error  $\Delta_d\sqrt{K}/\sigma \equiv \kappa$  versus  $\alpha^{-1}$ . The minimal exposure time needed to achieve a given enhancement  $\alpha$  is  $T(\alpha) = \tau K = \tau\kappa^2\alpha^2$ , where  $\tau$  is the luminescence lifetime. Notably, even under conditions that break Rayleigh's

curse ( $\kappa = \text{const}$ ), the exposure time  $T$  scales as  $T \propto \alpha^2$ , whereas for non-optimal imaging protocols, it scales as  $T \propto \alpha^4$ .

Under the selected experimental conditions, background noise has a greater impact than cross-talk. Therefore, Fig. 3h can be used to evaluate the applicability of our approach for real imaging scenarios, such as NV-centers ( $\tau = 10$  ns) localization. According to this plot, the BLESS protocol can achieve a 10-fold resolution enhancement in  $T(\alpha = 10) = 10$  ms, while the ESS protocol requires 1 s for the same enhancement. Thus, our approach enables at least a 10-fold resolution enhancement within feasible exposure times for real imaging experiments.

*Conclusion.*— In conclusion, we have introduced a novel imaging technique. Our method models the image with a few parameters, which are reconstructed by measuring the photon number distribution and modulating the target beam. Through rigorous analysis using Cramér–Rao bound theory (both classical and quantum) we have demonstrated, for the first time, the ability to break Rayleigh's curse in a realistic scenario involving two unbalanced single-photon emitters. The proposed technique holds significant potential for subdiffraction resolution in various fluorescence microscopy applications, ranging from the precise localization of NV-centers to broader bioimaging applications. Unlike other super resolution techniques such as STED and STORM/PALM, our method does not require luminescence switching off, thereby enabling its use with a wider range of fluorophores.

*Acknowledgements.*— We acknowledge useful discussions with Stanislav Straupe, Egor Kovlakov, Tatiana Smirnova, Stephen Vintskevich and René Reimann. This research was performed according to the MSU Program of Development, Project No 23-SCH06-05, and supported by the State Program no. FFNN-2022-0016 for Valiev Institute of Physics and Technology of RAS, and by the Russian Foundation for Basic Research (project no. 20-32-70153).

# Supplemental Material

This Supplementary document provides additional materials complementing the main text of the paper.

In Section , we present the derivation of distance estimation error based on statistical error propagation. Specifically, we derive equations (9) and (10) from the main text in Subsection and Subsection correspondingly.

In Section we define all the measurement protocols considered in the main text, in terms of Fisher information matrix.

Section offers additional analysis of cross-talk and background noise, illustrated in Fig 3(g,h) in the main text. In Subsection using statistical error propagation, we show that for the BLESS protocol, both imperfections significantly increase the distance estimation errors for  $d \ll d_c \equiv 2\sigma\sqrt{\frac{\mu_{bg} + \mu\chi}{\mu g}}$ . Similarly, in Subsection we demonstrate the robustness of the ESS protocol to both imperfections. Finally, in Subsection we confirm both statements by numerical CRB calculation at various values of background noise.

Section delves into additional materials related to quantum Fisher information (qFI) analysis. In subsection we offer a general description of the quantum state of light, created by two single-photon emitters in multiple frequency modes. In subsection we demonstrate that this quantum state yields identical results for photon number distribution measurements as presented in (4) in the main text. Then, in subsection we reduce this multi-mode state to the two-mode state, presented in (14) in the main text, and establish the equivalence of both states in terms of qFI. Finally, in subsection we provide some technical details regarding qFI calculation based on the two-mode state (14).

In Section , in addition to analytical approximations of  $d$  estimation errors presented in the inset of Fig. 3e in the main text, we present analytical approximations of estimation errors for all the model parameters.

## S1. Imaging protocols description, based on the propagation of statistical errors

### S1.1. Measure mean photon number in HG<sub>1</sub> mode

We begin by considering the measurement of the mean photon number in the HG<sub>1</sub> mode centered at the point  $x_D = x_c$ . In the small distance approximation ( $d \ll \sigma$ ), this mean photon number is approximated as:

$$M_{x_c} \equiv M_D^{(1)}(x_c) \approx \frac{\mu g d^2}{4\sigma^2}. \quad (S1)$$

Therefore, the distance  $d$  can be estimated as:

$$d = 2\sigma\sqrt{\frac{2M_{x_c}}{\mu g}}. \quad (S2)$$

Assuming accurate estimates of  $g$  and  $\mu$ , the distance estimation error  $\Delta_d$  is defined by the statistical errors of the measured mean photon number  $M_{x_c}$ . With  $\mu \ll 1$ , the mean photon number  $M_{x_c} \approx P_{1x_c} \equiv P_D^{(1)}(1|\theta, x_D = x_c)$ , and with a large number of measurements  $K \gg 1$ , the error becomes:

$$\Delta_{M_{x_c}}^2 = \Delta_{P_{1x_c}}^2 = \frac{P_{1x_c}}{K} = \frac{M_{x_c}}{K}. \quad (S3)$$

Finally, using (S3) and (S1), the distance estimation error is calculated as:

$$\Delta_d = \left| \frac{\partial d}{\partial M_{x_c}} \right| \Delta_{M_{x_c}} = \frac{d}{2M_{x_c}} \Delta_{M_{x_c}} = \frac{\sigma}{\sqrt{\mu g K}}, \quad (S4)$$

consistent with the equation (9) in the main text.

### S1.2. Measure two-photon probability in HG<sub>0</sub> mode

Next, we examine another example of imaging protocol, based on the measurement of photon statistics in the HG<sub>0</sub> mode centered at the points  $x_D = \pm\sigma$  assuming  $x_c \ll \sigma$  and  $d \ll \sigma$ . Then the probabilities to detect two photons are:

$$P_{2\pm} \equiv P_D^{(0)}(2|\theta, x_D) = \mu^2 g \frac{1 \pm 2x_c/\sigma \mp \gamma d/\sigma}{4e}. \quad (S5)$$

From these probabilities, parameters  $g$  and  $\gamma$  can be estimated as:

$$g = 2e \frac{P_{2+} + P_{2-}}{\mu^2}, \quad \gamma = \pm\sqrt{1 - g}, \quad (S6)$$

and the distance  $d$  can be estimated as:

$$d = 2 \frac{x_c}{\gamma} - \frac{2e\sigma}{\mu^2 g \gamma} (P_{2+} - P_{2-}). \quad (\text{S7})$$

Assuming accurate estimates of  $x_c$ ,  $\gamma$ , and  $\mu$ , the distance estimation error  $\Delta_d$  is determined by the statistical errors of the measured probabilities  $P_{2\pm}$ . With a large number of measurements  $K \gg 1$ , these errors become:

$$\Delta_{P_{2\pm}}^2 = \frac{P_{2\pm}}{K} \approx \frac{g\mu^2}{4eK}. \quad (\text{S8})$$

Finally, the distance estimation error is calculated as:

$$\Delta_d = \sqrt{\left(\frac{\partial d}{\partial P_{2+}}\right)^2 \Delta_{P_{2+}}^2 + \left(\frac{\partial d}{\partial P_{2-}}\right)^2 \Delta_{P_{2-}}^2} \approx 2\sqrt{2}e\sigma \frac{\Delta_{P_{2\pm}}}{\mu^2 g \gamma} \approx \sqrt{\frac{2e\sigma^2}{\mu^2 \gamma^2 g K}}, \quad (\text{S9})$$

equivalent to equation (10) in the main text.

## S2. Imaging protocols description, based on Fisher information matrix

In this section we define measurement protocols in terms of Fisher information matrix (FIM). See the definitions of FIM for full statistics measurements ( $F^{\text{stat}}$ ) and for mean photon number measurements ( $F^{\text{mean}}$ ) in the main text.

Since FIM is additive w.r.t. independent measurements, we define  $F_{\text{mesh}} = \frac{1}{11} \sum_{x_D \in \mathbf{X}_0} F_0(x_D)$ , where  $\mathbf{X}_0 = \{-1, -0.8, -0.6, \dots, 0.8, 1\}\sigma$  is the 11-points mesh scanning the sample in  $\text{HG}_0$ .

**Direct imaging (DI)** aims to extract the information from the intensity measurements in the standard  $\text{HG}_0$  mode, thus  $F_{\text{DI}} = K F_{\text{mesh}}^{\text{mean}}$ , where  $K$  is the total number of shots (proportional to the total exposition time).

With direct imaging, one can determine the centroid location  $\tilde{x}_c$  and then use the **SPADE protocol**: measure intensity at  $x_D = \tilde{x}_c$  in  $\text{HG}_1$ . To simplify analysis we choose the estimated location  $\tilde{x}_c$  as follows. The approximation of the mean photon number around  $x_c$  is

$$M_D^{(1)}(x_D) \approx \frac{\mu}{2\sigma^2} \left[ (x_D - x_c)^2 + \frac{gd^2}{2} \right], \quad (\text{S10})$$

The best information gain is obtained for the smallest value of  $M_D^{(1)}$ . Let us consider the case when the absolute error  $|\tilde{x}_c - x_c|$  of determining  $x_c$  at the first stage was small enough to make the first term in (S10) ten times smaller than the second one, i.e.,  $\tilde{x}_c = x_c + d\sqrt{g/20}$ . Suppose that both stages take  $K/2$  measurement samples, then  $F_{\text{SPADE}} = \frac{K}{2} (F_{\text{mesh}}^{\text{mean}} + F_1^{\text{mean}}(\tilde{x}_c))$ .

Due to the strong correlations between intensity ratio  $\gamma$  and distance  $d$ , above measurements are not enough to get a precise estimate of distance. In the main text we propose to measure the photon number distribution. **Estimating the shot statistics (ESS)** in points  $\mathbf{X}_0$  gives  $F_{\text{ESS}} = K F_{\text{mesh}}^{\text{stat}}$ . This measurement is enough to break Rayleigh's curse (the absolute estimation error becomes independent of  $d$ ), but the error remains quite high.

Thus, following SPADE, we complement the measurement protocol **BLESS** with additional intensity measurement of the modulated beam, resulting in  $F_{\text{BLESS}} = \frac{K}{2} (F_{\text{mesh}}^{\text{stat}} + F_1^{\text{mean}}(\tilde{x}_c))$ .

## S3. Cross-talk and background noise account

We address two main experimental imperfections. Firstly, non-ideal spatial modulation arises from imperfections in the spatial light modulator (SLM) and optical aberrations, leading to cross-talk between  $\text{HG}_0$  and  $\text{HG}_1$  modes. This results in a non-zero transmission coefficient  $\tilde{T}_s^{(1)} \Big|_{x_D=x_s} = \chi$ , modeled as  $\tilde{T}_s^{(1)} = \chi T_s^{(0)} + (1 - \chi) T_s^{(1)}$ .

Secondly, we consider background radiation with a Poissonian photon number distribution  $P_{\text{bg}}(k) = \frac{\mu_{\text{bg}}^k}{k!} e^{-\mu_{\text{bg}}}$ , characterized by mean photon number  $\mu_{\text{bg}}$ . Convolution with  $P_D^{(m)}(k)$  accounts for the total probability of detecting  $k$  photons  $\tilde{P}_D^{(m)}(k)$ . Assuming PNRD resolving up to two photons, we sum probabilities  $\tilde{P}_D^{(m)}(k \geq 2)$ .



### S3.1. Measure mean photon number in HG<sub>1</sub> mode

Let's first consider the measurement of the mean photon number in the HG<sub>1</sub> mode centered at the point  $x_D = x_c$ . In the small distance approximation ( $d \ll \sigma$ ), this mean photon number is given by Eq. (5,8) and is modified to account for background noise with mean photon number  $\mu_{\text{bg}}$  and spatial mode cross-talk  $\chi$ :

$$M_{x_c} \equiv M_D^{(1)}(x_c) \approx \frac{\mu g d^2}{4\sigma^2} + \mu_{\text{bg}} + \mu\chi. \quad (\text{S11})$$

Thus, the distance  $d$  can be estimated as:

$$d = 2\sigma \sqrt{2 \frac{M_{x_c} - \mu_{\text{bg}} - \mu\chi}{\mu g}}. \quad (\text{S12})$$

Assuming accurate estimates of  $g$  and  $\mu$ , we can use Eq. (S3) for  $\Delta_{M_{x_c}}$  and Eq. (S11) for  $M_{x_c}$  to estimate the distance error as:

$$\Delta_d = \left| \frac{\partial d}{\partial M_{x_c}} \right| \Delta_{M_{x_c}} = \frac{d \Delta_{M_{x_c}}}{2(M_{x_c} - \mu_{\text{bg}} - \mu\chi)} = \frac{\sigma}{\mu g d} \sqrt{\frac{\mu g d^2 + 4\sigma^2[\mu_{\text{bg}} + \mu\chi]}{K}}. \quad (\text{S13})$$

This equation shows that for  $d \gg d_c$ , where

$$d_c \equiv 2\sigma \sqrt{\frac{\mu_{\text{bg}} + \mu\chi}{\mu g}}, \quad (\text{S14})$$

the distance estimation error  $\Delta_d$  reduces to the initial case (S4). However, for  $d \ll d_c$ , the error increases as  $\Delta_d \propto d^{-1}$ :

$$\Delta_d \approx \frac{2\sigma^2}{\mu g d} \sqrt{\frac{\mu_{\text{bg}} + \mu\chi}{K}}, \quad (\text{S15})$$

indicating the return of Rayleigh's curse.

### S3.2. Measure two-photon probability in HG<sub>0</sub> mode

Now, considering the HG<sub>0</sub> mode measurements, we can neglect cross-talk, but background noise significantly alters the photon statistics. As was mentioned above, the total probability to detect  $k$  photons  $\tilde{P}_D^{(m)}(k)$  is the convolution of  $P_D^{(m)}(k)$  with Poisson distribution  $P_{\text{bg}}(k)$ . Thus, Eq. (4) for the probability distribution  $P_D^{(m)}(k|\theta, x_D)$  modifies as follows:

$$\tilde{P}_D^{(m)}(0) = P_{\text{bg}}(0)P_D^{(m)}(0) \quad (\text{S16a})$$

$$\tilde{P}_D^{(m)}(1) = P_{\text{bg}}(1)P_D^{(m)}(0) + P_{\text{bg}}(0)P_D^{(m)}(1) \quad (\text{S16b})$$

$$\tilde{P}_D^{(m)}(2) = 1 - \tilde{P}_D^{(m)}(0) - \tilde{P}_D^{(m)}(1) \quad (\text{S16c})$$

For measurements in the HG<sub>0</sub> mode centered at the points  $x_D = \pm\sigma$ , the probabilities to detect two photons under the assumptions  $d \ll \sigma$ ,  $x_c \ll \sigma$ ,  $\mu_{\text{bg}} \ll 1$  are:

$$P_{2\pm} \equiv P_D^{(0)}(2|\theta, x_D) = \mu \frac{\mu g (1 \pm 2x_c \mp d\gamma) + 4\sqrt{e}\mu_{\text{bg}}}{4e} \quad (\text{S17})$$

Hence, parameters  $g$  and  $\gamma$  can be estimated as:

$$g = 2\sqrt{e} \frac{\sqrt{e}(P_{2+} + P_{2-}) - 2\mu\mu_{\text{bg}}}{\mu^2}, \quad \gamma = \pm\sqrt{1-g}, \quad (\text{S18})$$

and the distance  $d$  can be estimated as:

$$d = 2\frac{x_c}{\gamma} - \frac{2e\sigma}{\mu^2 g \gamma} (P_{2+} - P_{2-}). \quad (\text{S19})$$

Since the equations (S19) and (S7) are the same, the background noise doesn't directly change the precision of  $d$  estimation, however it decrease the precision of  $g$  estimation due to the difference between (S18) and (S6) which indirectly slightly increase  $\Delta_d$ .



### S3.3. Cramér–Rao bound calculation

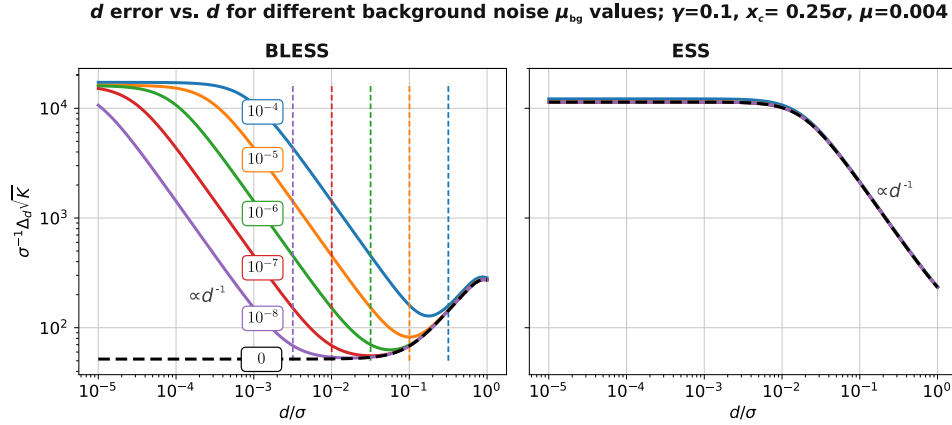


FIG. S1. Cramér–Rao bounds  $\Delta_d$  vs.  $d$  for ESS and BLESS protocols for different values of background noise  $\mu_{bg}$ . On the left (BLESS) plot, different colors correspond to different  $\mu_{bg}$  values. Corresponding values of  $d_c$  (S14) are plotted as vertical dashed lines. On the right (ESS) plot, different  $\mu_{bg}$  values correspond to the same colors as on the left one, but all the curves almost match.

The Cramér–Rao bounds for the ESS and BLESS protocols for different values of  $\mu_{bg}$  are presented in Fig S1. ESS, not requiring measurement in the  $HG_1$  mode, is robust to background noise and gives  $\Delta_d^{(ESS)}(d \rightarrow 0) \sim \sqrt{\frac{\sigma^2}{\mu^2 \gamma^2 g K}}$  for all  $\mu_{bg}$  values.

BLESS combines measurements in both  $HG_0$  and  $HG_1$  modes. For  $d \gg d_c$ , the estimation error  $\Delta_d^{(BLESS)} \sim \frac{\sigma}{\sqrt{\mu g K}}$  as in Eq. (S4), while for  $d \ll d_c$ , the error grows with decreasing  $d$  as  $\Delta_d^{(BLESS)} \sim \frac{\sigma^2}{\mu g d} \sqrt{\frac{\mu_{bg} + \mu x}{K}}$  until it reaches  $\Delta_d^{(BLESS)}(d \rightarrow 0) \sim \Delta_d^{(ESS)}(d \rightarrow 0) \sim \sqrt{\frac{\sigma^2}{\mu^2 \gamma^2 g K}}$ . In BLESS, half of the measurements being in  $HG_1$  mode, which adds no information about  $d$  at high background, leads to the bound  $\Delta_d^{(BLESS)}(d \rightarrow 0)$  larger than  $\Delta_d^{(ESS)}(d \rightarrow 0)$  by a factor of  $\sqrt{2}$ .

## S4. Quantum model of imaging

### S4.1. Image density operator

Let's consider a single-photon source  $S_s$  emitting a photon in the frequency mode  $\omega$  with probability  $\mu_s$ :

$$\hat{\rho}_s^{(\omega)} = (1 - \mu_s) |vac\rangle\langle vac| + \mu_s |\Psi_s\rangle\langle\Psi_s|_\omega, \quad (S20)$$

where  $|\Psi_s\rangle_\omega = \hat{A}_{s,\omega}^\dagger |vac\rangle$  and

$$\hat{A}_{s,\omega}^\dagger = \int dq \Psi_s(q) \hat{a}^\dagger(q, \omega). \quad (S21)$$

Let's assume the source emits a photon randomly into one of a large number of  $M$  different frequency modes, so  $\hat{\rho}_s = \frac{1}{M} \sum_\omega \hat{\rho}_s^{(\omega)}$ . For example, NV-centers in diamond emit photons together with a random number of phonons, and each phonon line is thermally broadened. The total number of spectral modes  $M$  can be estimated as a product of spectral bandwidth and luminescence lifetime, and for NV-centers,  $M \approx 6 \times 10^5$ .

For two sources  $S_a$  and  $S_b$ , one has

$$\begin{aligned} \hat{\rho}_M &= (1 - \mu_a)(1 - \mu_b) |vac\rangle\langle vac| \\ &+ \frac{\mu_a(1 - \mu_b)}{M} \sum_{\omega_a} \hat{A}_{a,\omega_a}^\dagger |vac\rangle\langle vac| \hat{A}_{a,\omega_a} \\ &+ \frac{\mu_b(1 - \mu_a)}{M} \sum_{\omega_b} \hat{A}_{b,\omega_b}^\dagger |vac\rangle\langle vac| \hat{A}_{b,\omega_b} \\ &+ \frac{\mu_a \mu_b}{M^2} \sum_{\omega_a, \omega_b} \frac{1}{N_{\omega_a \omega_b}} \hat{A}_{a,\omega_a}^\dagger \hat{A}_{b,\omega_b}^\dagger |vac\rangle\langle vac| \hat{A}_{a,\omega_a} \hat{A}_{b,\omega_b}. \end{aligned} \quad (S22)$$

Here  $N_{\omega_a\omega_b} = 1 + |V|^2 \delta_{\omega_a, \omega_b}$  is a normalization coefficient, and  $V = \langle \Psi_a | \Psi_b \rangle = \int dq \Psi_a^*(q) \Psi_b(q)$ . For the case  $M \gg 1$ , the probability of two sources simultaneously emitting a photon in the same mode  $\omega_a = \omega_b$  is negligible. Thus,

$$\hat{\rho}_M = \frac{1}{M(M-1)} \sum_{\omega_a \neq \omega_b} \hat{\rho}_a^{(\omega_a)} \hat{\rho}_b^{(\omega_b)} = \frac{1}{M(M-1)} \sum_{\omega_2 > \omega_1} \left[ \hat{\rho}_a^{(\omega_1)} \hat{\rho}_b^{(\omega_2)} + \hat{\rho}_b^{(\omega_1)} \hat{\rho}_a^{(\omega_2)} \right]. \quad (\text{S23})$$

An important property of this state is that one cannot measure the properties of a single source by filtering out some modes.

#### S4.2. Photon number measurements

Let's consider the single-source state  $\hat{\rho}_s^{(\omega)}$  (S20) measurement with PNRD in the detection mode  $\Phi(q) \equiv \Phi_0(q)$  on frequency  $\omega$ , where  $\Phi_m(q)$  is some set of orthogonal modes. For each mode  $m$ , one can introduce the Fock state basis  $\{|n_m\rangle_{m,\omega}\}$ . Since the detector measures mode  $m = 0$  only, let's take the partial trace over the rest modes:

$$\hat{\rho}_s^{(\omega, \Phi)} = \sum_{n_1, n_2, \dots = 0}^{\infty} \langle \{n_{m>0}\} | \hat{\rho}_s^{(\omega)} | \{n_{m>0}\} \rangle_{m>0, \omega}, \quad |\{n_{m>0}\}\rangle_{m>0, \omega} = \bigotimes_{m=1}^{\infty} |n_m\rangle_{m, \omega}. \quad (\text{S24})$$

Since the state  $\hat{\rho}_s^{(\omega)}$  contains up to one photon, this sum can be simplified as follows:

$$\hat{\rho}_s^{(\omega, \Phi)} = \langle 0 | \hat{\rho}_s^{(\omega)} | 0 \rangle_{m>0, \omega} + \sum_{m>0} \langle \tilde{1}_m | \hat{\rho}_s^{(\omega)} | \tilde{1}_m \rangle_{\omega}. \quad (\text{S25})$$

where  $|\tilde{1}_m\rangle_{\omega}$  is the state with one photon in the mode  $m$  and zero photons in rest of  $m > 0$  modes:

$$|\tilde{1}_m\rangle_{\omega} = \left[ \bigotimes_{m'=1}^{m-1} |0\rangle_{m', \omega} \right] |1\rangle_{m, \omega} \left[ \bigotimes_{m'=m+1}^{\infty} |0\rangle_{m', \omega} \right]. \quad (\text{S26})$$

Define  $T_s^{(m)} = |\langle \Psi_s | 1 \rangle_{m, \omega}|^2 = \left| \int \Psi_s^*(q) \Phi_m(q) dq \right|^2$ . One can easily find that

$$\langle 0 | \hat{\rho}_s^{(\omega)} | 0 \rangle_{m>0, \omega} = (1 - \mu_s) |0\rangle\langle 0|_{0, \omega} + \mu_s T_s^{(0)} |1\rangle\langle 1|_{0, \omega} \quad (\text{S27})$$

and

$$\langle \tilde{1}_m | \hat{\rho}_s^{(\omega)} | \tilde{1}_m \rangle_{\omega} = \mu_s T_s^{(m)} |0\rangle\langle 0|_{0, \omega}. \quad (\text{S28})$$

Since  $\sum_{m>0} T_s^{(m)} = 1 - T_s^{(0)}$ , after a few simplifications one finally obtains the detection mode density operator:

$$\hat{\rho}_s^{(\omega, \Phi)} = (1 - \mu_s T_s^{(0)}) |0\rangle\langle 0|_{\omega} + \mu_s T_s^{(0)} |1\rangle\langle 1|_{\omega} \quad (\text{S29})$$

Here we omitted the index of the mode  $m = 0$ . The above procedure is performed for each frequency mode  $\omega$ . Then, in analogy to (S23), one obtains the following density operator of two single photon sources in the detection mode  $\Phi$ :

$$\hat{\rho}_M^{(\Phi)} = \frac{1}{M(M-1)} \sum_{\omega_2 > \omega_1} \left[ \rho_a^{(\omega_1, \Phi)} \rho_b^{(\omega_2, \Phi)} + \rho_b^{(\omega_1, \Phi)} \rho_a^{(\omega_2, \Phi)} \right]. \quad (\text{S30})$$

Consider a PNRD that does not resolve different frequency modes. Such a PNRD would have the following POVM effects:

$$\hat{E}_0 = |0\rangle\langle 0|, \quad \hat{E}_1 = \sum_{\omega} |1\rangle\langle 1|_{\omega}, \quad \hat{E}_2 = I - \hat{E}_0 - \hat{E}_1. \quad (\text{S31})$$

One can easily verify, that  $P_D(k) = \text{Tr}(\hat{E}_k \hat{\rho}_M^{(\Phi)})$  is equal to the classical distribution Eq. (4) from the main text.

#### S4.3. Two-mode state

The state  $\hat{\rho}_M$  (S23) can be reduced to a two-mode state as follows. Consider an arbitrary POVM  $\{\hat{E}_k : \hat{E}_k \geq 0, \sum_k \hat{E}_k = I\}$ . The corresponding probabilities are:

$$p_k = \text{Tr}(\hat{E}_k \hat{\rho}_M) = \frac{1}{M(M-1)} \sum_{\omega_2 > \omega_1} \text{Tr} \left( \hat{E}_k \left[ \hat{\rho}_a^{(\omega_1)} \hat{\rho}_b^{(\omega_2)} + \hat{\rho}_b^{(\omega_1)} \hat{\rho}_a^{(\omega_2)} \right] \right). \quad (\text{S32})$$

For each term in the right-hand side, let's first take the trace over the modes with  $\omega \neq \omega_1, \omega_2$ . Since the states in these modes are all vacuum states, one can introduce the operator

$$\hat{E}_{k,\omega_1,\omega_2}^{(\omega_1,\omega_2)} = \left[ \bigotimes_{\omega \neq \omega_1, \omega_2} \langle vac |_\omega \right] \hat{E}_k \left[ \bigotimes_{\omega \neq \omega_1, \omega_2} | vac \rangle_\omega \right] \quad (S33)$$

that acts in the subspace of modes  $\omega_1$  and  $\omega_2$ . The trace over the rest modes  $\omega_1$  and  $\omega_2$  is then

$$p_k = \frac{1}{M(M-1)} \sum_{\omega_2 > \omega_1} \text{Tr}_{\omega_1, \omega_2} \left( \hat{E}_{k,\omega_1,\omega_2}^{(\omega_1,\omega_2)} \left[ \hat{\rho}_a^{(\omega_1)} \hat{\rho}_b^{(\omega_2)} + \hat{\rho}_b^{(\omega_1)} \hat{\rho}_a^{(\omega_2)} \right] \right). \quad (S34)$$

Note that for any pair of modes  $\omega_1$  and  $\omega_2$ , the corresponding two-mode state is the same and equal to Eq. (14) in the main text:

$$\hat{\rho}_2 = \frac{1}{2}(\hat{\rho}_a \otimes \hat{\rho}_b + \hat{\rho}_b \otimes \hat{\rho}_a), \quad (S35)$$

Thus, one can separately take the sum over two-mode operators  $\hat{E}_{k,\omega_1,\omega_2}$  as follows:

$$\hat{E}_{2,k} = \frac{2}{M(M-1)} \sum_{\omega_2 > \omega_1} E_{k,\omega_1,\omega_2}. \quad (S36)$$

and obtain  $p_k = \text{Tr}(\hat{E}_{2,k} \hat{\rho}_2)$ . Using the definition (S33) one can verify that  $\hat{E}_{2,k} \geq 0$  for all  $k$ , and that  $\sum_k \hat{E}_{2,k} = I$ . Thus, operators  $\{\hat{E}_{2,k}\}$  also form valid POVM effects. Moreover, if one takes effects  $\hat{E}_k$  such that they maximize the Fisher information over the parameters encoded in  $\rho_a$  and  $\rho_b$ , the operators  $\hat{E}_{2,k}$  would also maximize it. Thus, the quantum Fisher information for the states  $\hat{\rho}_M$  and  $\hat{\rho}_2$  is also the same.

#### S4.4. Computing quantum Fisher information

The computation of the quantum Fisher information matrix for the state  $\hat{\rho}_2$  (14) is complicated due to the infinite number of spatial modes, each containing 0 or 1 photons. However, one can reduce the task by finding a minimal orthogonal basis that supports  $\hat{\rho}_2$  and its derivatives. Following the main text, we define the single photon state emitted from the source  $S_s$  as

$$|\Psi_s\rangle = \int dq \Psi_s(q) a^\dagger(q) |vac\rangle, \quad \Psi_s(q) = \sqrt{\frac{\sigma}{\sqrt{\pi}}} e^{-\frac{\sigma^2 q^2}{2}} e^{-iqx_s}. \quad (S37)$$

The partial derivative of this state with respect to some parameter  $\theta$  is related to the HG<sub>1</sub> mode:

$$\partial_\theta |\Psi_s\rangle = \frac{\partial_\theta x_s}{\sqrt{2}\sigma} |\bar{\Psi}_s\rangle, \quad (S38)$$

where

$$|\bar{\Psi}_s\rangle = \int dq \bar{\Psi}_s(q) a^\dagger(q) |vac\rangle, \quad \bar{\Psi}_s(q) = \sqrt{\frac{\sigma}{\sqrt{\pi}}} e^{-\frac{\sigma^2 q^2}{2}} e^{-iqx_s} (-i\sqrt{2}\sigma q). \quad (S39)$$

Thus, the derivative of the single-source state  $\hat{\rho}_s = (1 - \mu_s) |vac\rangle\langle vac| + \mu_s |\Psi_s\rangle\langle\Psi_s|$  with respect to the parameter  $\theta$  is

$$\partial_\theta \hat{\rho}_s = \partial_\theta \mu_s (|\Psi_s\rangle\langle\Psi_s| - |vac\rangle\langle vac|) + \frac{\mu_s \partial_\theta x_s}{\sqrt{2}\sigma} (|\Psi_s\rangle\langle\bar{\Psi}_s| + |\bar{\Psi}_s\rangle\langle\Psi_s|) \quad (S40)$$

The derivative of the two-mode state (S35) is

$$\partial_\theta \hat{\rho}_2 = \frac{1}{2} ((\partial_\theta \hat{\rho}_a) \otimes \hat{\rho}_b + \hat{\rho}_a \otimes (\partial_\theta \hat{\rho}_b) + (\partial_\theta \hat{\rho}_b) \otimes \hat{\rho}_a + \hat{\rho}_b \otimes (\partial_\theta \hat{\rho}_a)). \quad (S41)$$

One can observe that for  $\hat{\rho}_2$  and  $\partial_\theta \hat{\rho}_2$  each mode is supported by the set of five states

$$\{|vac\rangle, |\Psi_a\rangle, |\Psi_b\rangle, |\bar{\Psi}_a\rangle, |\bar{\Psi}_b\rangle\}. \quad (S42)$$

Following [5] (Appendix C), we introduce an orthonormal basis  $\{|e_k\rangle, k = 0, \dots, 4\}$  such that

$$\begin{aligned} |vac\rangle &= |e_0\rangle, & |\Psi_a\rangle &= a_+ |e_1\rangle + a_- |e_2\rangle, & |\Psi_b\rangle &= a_+ |e_1\rangle - a_- |e_2\rangle, \\ |\bar{\Psi}_a\rangle &= -b_+ |e_1\rangle + b_- |e_2\rangle + c_- |e_3\rangle + c_+ |e_4\rangle, \\ |\bar{\Psi}_b\rangle &= +b_+ |e_1\rangle + b_- |e_2\rangle + c_- |e_3\rangle - c_+ |e_4\rangle, \end{aligned} \quad (S43)$$

where

$$a_{\pm} = \sqrt{\frac{1 \pm V}{2}}, \quad b_{\pm} = \frac{d}{\sqrt{8}\sigma a_{\pm}} V, \quad c_{\pm} = \sqrt{a_{\mp}^2 \pm \frac{b_{\pm}^2}{V}}, \quad (\text{S44})$$

and  $V = e^{-\frac{d^2}{4\sigma^2}}$ . Having this decomposition we define  $\hat{\rho}_2$  and  $\partial_{\theta}\hat{\rho}_2$  in the matrix representation and then compute the quantum Fisher information matrix numerically.

## S5. Comparison of error bounds

	$K\Delta_d^2$	$K\Delta_{\gamma}^2$	$K\Delta_{x_c}^2$	$K\Delta_{\mu}^2$
ESS	$\frac{19.3\sigma^2}{\gamma^2 g \mu^2}$	$\frac{1.5g}{\gamma^2 \mu^2}$	$\frac{3.5\sigma^2}{\mu}$	$1.2\mu$
BLESS	$\frac{10.5\sigma^2}{g\mu}$	$\frac{2.8g}{\gamma^2 \mu^2}$	$\frac{7.0\sigma^2}{\mu}$	$2.4\mu$
qCRB-2	$\frac{2\sigma^2}{g\mu}$	$\frac{g}{\gamma^2 \mu^2}$	$\frac{\sigma^2}{2\mu}$	$\mu$

TABLE S1. Estimation variances of all the model parameters at the limit  $d \rightarrow 0$ , assuming  $x_c \ll \sigma$  and  $\mu \ll 1$ .

In Table S1, we present the semi-analytical equations for parameters' estimation variances at the limit  $d \rightarrow 0$  and for small values of  $x_c$  and  $\mu$ . One can see that for all the parameters except  $d$ , both ESS and BLESS protocols have similar (up to a constant factor) values of estimation variances as qCRB-2. However, only the BLESS protocol can reach qCRB-2 for distance estimation. The ESS protocol gives a distance variance of  $\gamma^{-2}\mu^{-1}$  times bigger.

---

\* k.g.katamadze@gmail.com

- [1] F. R. S. Rayleigh, Xxi. investigations in optics, with special reference to the spectroscope, The London, Edinburgh, and Dublin Philosophical Magazine and Journal of Science **8**, 261–274 (1879).
- [2] T. Müller, C. Schumann, and A. Kraegeloh, Sted microscopy and its applications: New insights into cellular processes on the nanoscale, ChemPhysChem **13**, 1986–2000 (2012).
- [3] M. J. Rust, M. Bates, and X. Zhuang, Sub-diffraction-limit imaging by stochastic optical reconstruction microscopy (storm), Nature Methods **3**, 793–796 (2006).
- [4] E. Betzig, G. H. Patterson, R. Sougrat, O. W. Lindwasser, S. Olenych, J. S. Bonifacino, M. W. Davidson, J. Lippincott-Schwartz, and H. F. Hess, Imaging intracellular fluorescent proteins at nanometer resolution, Science **313**, 1642–1645 (2006).
- [5] M. Tsang, R. Nair, and X.-M. Lu, Quantum theory of superresolution for two incoherent optical point sources, Physical Review X **6**, 031033 (2016).
- [6] R. Nair and M. Tsang, Interferometric superlocalization of two incoherent optical point sources, Optics Express **24**, 3684 (2016).
- [7] R. Nair and M. Tsang, Far-field superresolution of thermal electromagnetic sources at the quantum limit, Physical Review Letters **117**, 190801 (2016).
- [8] M. Paúr, B. Stoklasa, Z. Hradil, L. L. Sánchez-Soto, and J. Rehacek, Achieving the ultimate optical resolution, Optica **3**, 1144 (2016).
- [9] W.-K. Tham, H. Ferretti, and A. M. Steinberg, Beating rayleigh's curse by imaging using phase information, Physical Review Letters **118**, 070801 (2017).
- [10] M. Paúr, B. Stoklasa, J. Grover, A. Krzic, L. L. Sánchez-Soto, Z. Hradil, and J. Řeháček, Tempering rayleigh's curse with psf shaping, Optica **5**, 1177 (2018).
- [11] J. M. Donohue, V. Ansari, J. Řeháček, Z. Hradil, B. Stoklasa, M. Paúr, L. L. Sánchez-Soto, and C. Silberhorn, Quantum-Limited Time-Frequency Estimation through Mode-Selective Photon Measurement, Physical Review Letters **121**, 1 (2018), arXiv:1805.02491.
- [12] P. Boucher, C. Fabre, G. Labroille, and N. Treps, Spatial optical mode demultiplexing as a practical tool for optimal transverse distance estimation, Optica **7**, 1621 (2020).
- [13] K. A. G. Bonsma-Fisher, W.-K. Tham, H. Ferretti, and A. M. Steinberg, Realistic sub-rayleigh imaging with phase-sensitive measurements, New Journal of Physics **21**, 093010 (2019).
- [14] J. Řeháček, Z. Hradil, B. Stoklasa, M. Paúr, J. Grover, A. Krzic, and L. L. Sánchez-Soto, Multiparameter quantum metrology of incoherent point sources: Towards realistic superresolution, Physical Review A **96**, 062107 (2017).
- [15] S. W. Hell, J. Soukka, and P. E. Hänninen, Two- and multiphoton detection as an imaging mode and means of increasing the resolution in far-field light microscopy: A study based on photon-optics, Bioimaging **3**, 64 (1995).

- [16] O. Schwartz and D. Oron, Improved resolution in fluorescence microscopy using quantum correlations, *Phys. Rev. A* **85**, 33812 (2012).
- [17] O. Schwartz, J. M. Levitt, R. Tenne, S. Itzhakov, Z. Deutsch, and D. Oron, Superresolution microscopy with quantum emitters., *Nano Lett.* **13**, 5832–5836 (2013).
- [18] D. Gatto Monticone, K. Katamadze, P. Traina, E. Moreva, J. Forneris, I. Ruo-Berchera, P. Olivero, I. P. Degiovanni, G. Brida, and M. Genovese, Beating the abbe diffraction limit in confocal microscopy via nonclassical photon statistics, *Physical Review Letters* **113**, 143602 (2014).
- [19] R. Tenne, U. Rossman, B. Rephael, Y. Israel, A. Krupinski-Ptaszek, R. Lapkiewicz, Y. Silberberg, and D. Oron, Super-resolution enhancement by quantum image scanning microscopy, *Nature Photonics* **13**, 116 (2019), arXiv:1806.07661.
- [20] R. A. Bartels, G. Murray, J. Field, and J. Squier, Super-Resolution Imaging by Computationally Fusing Quantum and Classical Optical Information, *Intelligent Computing* **2022**, 1 (2022).
- [21] Z. A. Kudyshev, D. Sychev, Z. Martin, O. Yesilyurt, S. I. Bogdanov, X. Xu, P.-G. Chen, A. V. Kildishev, A. Boltasseva, and V. M. Shalaev, Machine learning assisted quantum super-resolution microscopy, *Nature Communications* **14**, 4828 (2023).
- [22] Y. Israel, R. Tenne, D. Oron, and Y. Silberberg, Quantum correlation enhanced super-resolution localization microscopy enabled by a fibre bundle camera, *Nature Communications* **8**, 14786 (2017), arXiv:1609.00312.
- [23] J. G. Worboys, D. W. Drumm, and A. D. Greentree, Quantum multilateration: Subdiffraction emitter pair localization via three spatially separate Hanbury Brown and Twiss measurements, *Physical Review A* **101**, 13810 (2020).
- [24] A. Sroda, A. Makowski, R. Tenne, U. Rossman, G. Lubin, D. Oron, and R. Lapkiewicz, SOFISM: Super-resolution optical fluctuation image scanning microscopy, *Optica* **7**, 1308 (2020), arXiv:2002.00182.
- [25] S. Li, W. Li, Q. Sun, B. Moran, T. C. Brown, B. C. Gibson, and A. D. Greentree, Localising two sub-diffraction emitters in 3D using quantum correlation microscopy, *New Journal of Physics* **26**, 033036 (2024), arXiv:2310.02585.
- [26] See Supplemental Material for more information.
- [27] M. G. Kendall and A. Stuart, *The Advanced Theory of Statistics, Vol. 2: Inference and Relationship* (Charles Griffin and Company Ltd., 1961).
- [28] H. Cramér, *Mathematical Methods of Statistics* (Princeton University Press, 1999).
- [29] E. Bisketzi, D. Branford, and A. Datta, Quantum limits of localisation microscopy, *New Journal of Physics* **21**, 123032 (2019).
- [30] J. Liu, H. Yuan, X.-M. Lu, and X. Wang, Quantum fisher information matrix and multiparameter estimation, *Journal of Physics A: Mathematical and Theoretical* **53**, 023001 (2020).
- [31] L. Peng and X. M. Lu, Generalization of rayleigh’s criterion on parameter estimation with incoherent sources, *Physical Review A* **103**, 1–10 (2021).
- [32] M. Paúr, B. Stoklasa, D. Koutný, J. Řeháček, Z. Hradil, J. Grover, A. Krzic, and L. L. Sánchez-Soto, Reading out fisher information from the zeros of the point spread function, *Optics Letters* **44**, 3114 (2019).
- [33] B. E. Svensson, Pedagogical review of quantum measurement theory with an emphasis on weak measurements, *Quanta* **2**, 18 (2013).
- [34] G. Struchalin, E. Kovlakov, S. Straupe, and S. Kulik, Adaptive quantum tomography of high-dimensional bipartite systems, *Physical Review A* **98**, 032330 (2018).
- [35] S. Bogdanov, S. Bolshedvorskii, A. Zeleneev, V. Soshenko, O. Rubinas, D. Radishev, M. Lobaev, A. Vikharev, A. Gorbachev, M. Drozdov, *et al.*, Optical investigation of as-grown nv centers in heavily nitrogen doped delta layers in cvd diamond, *Materials Today Communications* **24**, 101019 (2020).
- [36] L. Santamaria, D. Pallotti, M. S. de Cumis, D. Dequal, and C. Lupo, Spatial-mode demultiplexing for enhanced intensity and distance measurement, *Optics Express* **31**, 33930 (2023).